

Phenomenology of renormalization group improved gravity from the kinematics of SPARC galaxies.

Esha Bhatia,^a Sayan Chakrabarti,^a Sovan Chakraborty^a

^aIndian Institute of Technology, Guwahati, India

E-mail: b.asha@iitg.ac.in, sayan.chakrabarti@iitg.ac.in, sovan@iitg.ac.in

Abstract. Renormalization Group correction to General Relativity (RGGR) proposes a logarithmic running of the gravitational coupling (G), resulting in a modified description of gravity. This has the potential to explain the observed kinematics of the galaxies including the missing-mass problem. We, for the first time, based on the galaxy morphological types, investigate the dynamics of a diverse collection of galaxies present in the Spitzer Photometry for Accurate Rotation Curve (SPARC) catalog. We phenomenologically constrain the RGGR model parameter ($\bar{\nu}$) along with the mass-to-light ratio for a sample of 100 SPARC galaxies, selected from four different morphological types, viz. early, spiral, late, and starburst. Our statistical analysis finds RGGR to fit the observed galaxy kinematics consistently. The constrained RGGR model parameter also supports the claim that it has a near-linear dependence on the galactic baryonic mass. From our morphology study, we find that the parameter $\bar{\nu}$ decreases from the early-type to the starburst galaxies. Finally, the renormalization group improved gravity is tested against the two established empirical relations for the SPARC catalog, viz., the Radial Acceleration Relation (RAR) and the Baryonic Tully Fisher relation (BTFR), both are found to satisfy consistently.

Contents

1	Introduction	1
2	RGGR gravity model	3
3	Galaxy catalogue	4
4	Methodology	7
5	Results	8
5.1	Fit to the observed Rotation Curve	10
5.2	Relation of \bar{v} with baryonic matter	16
5.3	Empirical relations for SPARC	17
5.3.1	Radial Acceleration Relation (RAR)	17
5.3.2	Baryonic Tully Fisher Relation (BTFR)	18
6	Conclusion	19

1 Introduction

The proposal to modify the action of the general theory of relativity (GR) has been found to be successful [1, 2] in mitigating the missing-mass problem [3, 4, 5]. This leads to the introduction of additional components such as scalar, vector, or tensor fields in the action of gravity [1, 2, 6]. On the other hand, the dark matter (DM) explanation to these galactic kinematic issues is found to have wider implications in cosmology and astroparticle physics [7, 8, 9]. Although both modified gravity and DM scenarios are appealing, they suffer from certain challenges and shortcomings. On one hand, we have Λ CDM [7], which has issues such as core-cusp problem [10], coincidence problem [11], missing satellite problem [12, 13] and many more [7, 14, 15, 16]. Similarly, any modified theory of gravity must demonstrate stability throughout all epochs of cosmic evolution without exhibiting any internal instabilities within its framework [1, 17, 18]. Consequently, the detection of gravitational waves has led to the exclusion of several alternative theories that were inconsistent with the obtained phenomenological constraint on the mass of the graviton [19, 20]. Keeping all the past references in mind, our work in this paper discusses an alternative gravity scenario, which can explain the rotation curve for a large selection of galaxies. Specifically, we look into a model that studies the effect of the renormalization group (RG) running on the parameters under quantum field theory in curved spacetime.

Renormalization Group correction to General Relativity (RGGR) proposes running of the gravitational coupling (G) with the energy scale [21, 22, 23] and has been found to provide an alternative description to the galactic kinematic discrepancies [24, 25, 26]. The previous studies on the RG effect showed that a logarithmic running of G can phenomenologically explain the kinematics of galaxies [21, 27]. Additionally, the energy scale of the running parameter is related to the observable potential with the condition that it must satisfy the Tully-Fisher relation and regain the correct Newtonian limit on Solar system scales [28, 29] as well as on

astrophysical scales [30]. Similarly, earlier work on the RG study also accounts for the renormalization running of the cosmological constant (Λ) [28, 31]. However, due to the smallness of Λ , any modification arising out of the running of Λ can be neglected on the galactic scales [25, 26, 29]. The running of the gravitational constant results in a phenomenological parameter ($\bar{\nu}$) for the RGGR model. Studies on the kinematics of spiral and elliptical galaxies show that the $\bar{\nu}$ is of the order of 10^{-7} [25, 29, 32]. The parameter $\bar{\nu}$, which determines the strength of the running, has been found to have an almost linear relation with the baryonic mass of the galaxy and has been studied for a number of galaxies [29]. In the following, we analyze the RGGR model with an even larger selection of galactic rotation curve (RC), as compiled in the Spitzer Photometry for Accurate Rotation Curve (SPARC) [33].

SPARC [33] is a collection of 175 rotationally supported galaxies that contain the radial variation of net circular velocity, measured at near-infrared region. This catalog has been extensively used for the phenomenological study of a large number of DM [34, 9] and alternative gravity models [35, 36, 37]. In addition to the net circular velocity, the catalog compiles the mass modeling of individual baryonic components, viz., disk, bulge, and gas of the galaxy. The SPARC encompasses galaxies belonging to different morphological types. This includes galaxies ranging from Hubble type 0 – 12 that consist of Early, Spiral, Late-type, and Starburst galaxies. Our analysis of the RGGR model extends to all 4 morphological types. We aim to study the dependence of the alternative gravity parameter on the galaxy morphology, and in this regard, we, for the first time, based on the galaxy morphological types, investigate the dynamics of a diverse collection of galaxies.

SPARC imposes certain selection criteria on the quality of observational data and the inclination of the galaxies from our reference frame, which reduces the number of relevant galaxies to 153. Additionally, we impose a χ^2 cutoff to ensure that our analysis of the RGGR model shows a consistent fit with the observations. This further reduces the number of relevant galaxies to 100. For each of these 100 galaxies, we constrain the RGGR parameter $\bar{\nu}$ from the observed RC data. The linear dependence of the parameter $\bar{\nu}$ for a wide range of masses in SPARC galaxies ($10^8 - 10^{11} M_\odot$) is also determined in our analysis. The model parameters of the individual galaxies are statistically constrained using an algorithm based on the Bayesian technique known as Markov Chain Monte Carlo (MCMC) [38]. We also report the goodness of fit of individual galaxies by measuring the χ^2 value to explain the consistency of the gravity model.

We extend the phenomenology of the RGGR model further to the well-known empirical relations, the Radial Acceleration Relation (RAR) and the Baryonic Tully-Fisher Relation (BTFR). Independent of the underlying gravity model, an analytical relation exists between the observed and baryonic accelerations for all the SPARC galaxies. This relation is known as RAR [39], which hints towards modified kinematics that govern the motion on galactic scales. Another such relation, known as the BTFR [40, 41] signifies that the baryonic mass contained within all the galaxies present in the SPARC catalog has a power-law dependence on the flat part of the circular velocity (V_f) far from the galactic center. Using the best-fit values obtained from the RC analysis with the emcee sampler, we establish the above two relations of the SPARC catalog. As both the relations were evaluated from the observational data, having no model dependence, such relations become a consistency check for the gravity model used. Our elaborate analysis aims to check the consistency of the RGGR model for a

rather large selection of rotationally supported galaxies to date.

The layout of the paper is as follows. Section 2 gives a detailed account of the RGGR model. The next Section 3 discusses in detail the galaxy catalog SPARC adopted for studying the alternative gravity model. The methodology and the computational packages used to sample the parameter space of the model are discussed in Section 4. The following Section 5 and Section 6 discuss the results obtained and the conclusion for our study, respectively.

2 RGGR gravity model

Renormalization Group correction to General Relativity is a quantum gravity model that studies the variation of the gravitational coupling parameter (G) with the energy scale of the Universe [21, 23, 24]. The observations in the far infrared region established G to be a constant in nature. However, this might not be true if one looks at GR as a field theory in curved spacetime. The beta function for the gravitational coupling constant G has been studied to have a logarithmic dependence on the energy scale (μ) of the Universe. From the dimensional argument, one unique choice for the beta function has been taken to be of the following form [23, 24]

$$\beta = \mu \frac{dG^{-1}}{d\mu} = 2\nu \frac{M_{planck}^2}{c\hbar} = 2\nu G_0^{-1}, \quad (2.1)$$

where ν is a phenomenological parameter that is fixed from observational data, and G_0 is the bare value of the gravitational coupling parameter. The logarithmic dependence of G with the energy scale as obtained from the solution of Eq.2.1 becomes

$$G(\mu) = \frac{G_0}{1 + \nu \ln\left(\frac{\mu^2}{\mu_0^2}\right)}, \quad (2.2)$$

here μ_0 is the energy scale defined such that $G(\mu_0) = G_0$. As the variation in G is small, the exact value of μ_0 is inconsequential. For the far-infrared (IR) region, where the coupling parameter G is known to be a constant, the GR limit is regained by substituting $\nu = 0$. Thus, the coupling parameter G in the Einstein-Hilbert action of gravity follows the RG flow given in Eq.2.2. For observations in galactic scales the variation in ν is of the order 10^{-7} [29]. A similar β function can also be defined for the cosmological constant ($\Lambda(\mu)$) present in the action of gravity. However, due to the negligible effect on the astrophysical scales, it is ignored from the RC analysis of the galaxies [24].

Additionally, to formulate a consistent theory with an observational basis, it is required to correlate the energy scale with some observable parameter. For example, on the cosmological scales, μ is shown to have a relation with the energy scale of the Universe i.e., Hubble constant (H) [27]. Similarly, for the galactic scales, μ has a functional dependence on the potential energy of the system. The relation between the energy scale dependence of the parameter with the potential is defined such that it regains the correct Newtonian limit and satisfies the Tully Fisher relation. Thus, the functional form that satisfies the mentioned condition can be assumed to be [27]

$$\frac{\mu}{\mu_0} = \left(\frac{\phi}{\phi_0}\right)^\alpha, \quad (2.3)$$

where α is a phenomenological parameter constrained from the observations. The analysis of galactic dynamics with RGGR [25, 29] suggests that the parameter $\nu\alpha \equiv \bar{\nu}$ follows a close to linear relation with the baryonic mass of the galaxy. Such a linear relation has been shown from the study of RC of spiral galaxies [29] and from the fundamental plane of elliptical galaxies [25]. Solving for the weak-field limit, the effective circular velocity and acceleration take the following forms [24, 25]

$$V_{RGGR}(r)^2 = V_N(r)^2 \left(1 - \frac{c^2 \bar{\nu}}{\phi_N(r)} \right), \quad (2.4)$$

$$a_{RGGR}(r) \approx a_N(r) \left(1 - \frac{c^2 \bar{\nu}}{\phi_N(r)} \right), \quad (2.5)$$

where $V_N(r)$ and $a_N(r)$ are the Newtonian contribution to the velocity and acceleration, respectively, c is the speed of light. Thus, on the galactic scales, the net circular velocity and acceleration of an object in addition to the Newtonian (baryonic) part have the extra contribution due to the modified gravity. This extra contribution depends on the model parameter $\bar{\nu}$ and the potential $\phi_N(r)$. The potential $\phi_N(r)$ arises from all the baryonic contents of the galaxy and is crucial to evaluate the effect of RGGR gravity. This requires mass modeling, i.e., modeling the radial dependence of the baryonic mass of the galaxy. In general, the baryonic structure of the galaxy is composed of three components, i.e., disk, gas, and bulge. We assume a radial exponential profile [42] for the disk and gas component. For the galaxies having bulge, the mass modeling is done assuming a spheroidal Hernquist profile [43]. Thus, for the given mass profiles, one may estimate or constrain the phenomenological parameter $\bar{\nu}$ from observations. For example, rotation curve studies [29] estimate $\bar{\nu}$ to be of the order of 10^{-7} to be consistent with the observations.

Additionally, the constraints obtained on the solar system scales suggest the parameter $\bar{\nu}$ to be of the order of 10^{-17} [23]. The limit is much smaller than the galaxy rotation curve estimates. This, however, is expected as the parameter $\bar{\nu}$ is found to have a linear dependence on the baryonic mass of the system. In comparison to the spiral galaxies, the mass contained within the Solar system is about ten times less, thus making the $\bar{\nu} \sim 10^{-17}$ limit consistent. Similarly, in the case of Ultra-diffuse galaxies, whose masses are comparatively smaller than the rotationally supported galaxies, the evaluated $\bar{\nu}$ turns out to be 10^{-8} [44]. In what follows, we analyze the consistency of the RGGR model for a large selection of galaxies from the SPARC catalog. These galaxies belonging to different morphologies with different characteristics give a measure of the model parameter's variation over the nature of the galaxies.

3 Galaxy catalogue

Spitzer Photometry for Accurate Rotation Curve (SPARC) contains the collection of 175 rotationally supported galaxies measured at near-IR photometry [33]. The catalog contains the mass models of galaxies covering a broad range with varying luminosities, morphologies, rotation velocity, gas content, etc. [33]. The dominant contribution for a rotationally supported galaxy comes from the disk, which extends up to a few kiloparsecs. The additional baryonic contribution arises from the bulge (if present) superimposed at the disk's center and gas diffused throughout the galaxy. Depending upon the size of the bulge and structure of

spiral arms present, the SPARC is majorly divided into 4 morphological types. The different morphologies are represented via Hubble type (H), which for the catalog ranges between $H : 0 - 12$ [45]. The Hubble type is a representation of the evolutionary stage of the galaxy. In general, the size of the bulge and tightness of spiral arms for a rotationally supported galaxy reduces as we move up in the Hubble type. The first Hubble category ranging from $H : 0 - 2$ belongs to the Early type, which contains galaxies of type S0, Sa, and Sab, respectively. Such galaxies are distinguished by the presence of a prominent bulge at the center and tightly woven spiral arms. The second category consists of Spiral galaxies ($H : 3 - 6$) where the features such as bulge and tightness of spiral arms start decreasing. The next two categories include Late-type ($H : 7 - 9$) and Starburst ($H : 10 - 12$). These galaxies contain almost no visible bulge present at the center of the galaxy. The last category i.e., Starburst galaxies are known to have no spiral structure in the outer parts and are characterized by their diffused shape. The Starburst galaxies are also known to have a higher star formation rate. Thus, this catalog represents a wide spectrum of galaxies and makes a versatile ground to test our alternative gravity model.

Rotation Curve: Given the radial variation of the velocity for individual baryonic components of a galaxy, the total Newtonian contribution can be written as:

$$v_N^2(r) = \gamma_d v_{disk}^2(r) + \gamma_b v_{bulge}^2(r) + |v_{gas}(r)| v_{gas}(r); \quad (3.1)$$

where $v_{disk}(r)$, $v_{bulge}(r)$ and $v_{gas}(r)$ represent the disk, bulge, and gas velocity components for a particular galaxy in the SPARC catalog. The radial variation of the individual baryonic component for each rotationally supported galaxy is provided within the SPARC. The catalog additionally contains the accurate HI and H α measurement of the total circular velocity $v_{obs}(r)$, along with the error bars $\sigma(r)$ for every galaxy. Also, the two baryonic components are scaled by a factor γ_d and γ_b , which measure the mass-to-light ratio for the disk and bulge part, respectively. The data from the catalog clearly shows that the net contribution of velocity coming from the baryonic component is insufficient to explain the observed velocity, $v_{obs}(r)$ of the galaxy. This leaves room for the additional components, such as DM or MOG which can be added to the Newtonian part to explain the overall rotational stability of the galaxy.

Under the assumption that the gravity on the galactic scale is RGGR, the modified kinematics of objects within the galaxy is expressed as given in Eq.2.4. The equation shows that the net circular velocity has an additional contribution from the RGGR gravity. Therefore, comparing the total observed circular velocity from the SPARC catalog with the RGGR velocity form (Eq.2.4) helps to check the consistency of the gravity model. This requires the variation of the model parameter of the theory within the allowed parameter space. This analysis aims to look for the parameters that give a consistent fit to the observed RC of the galaxy sample. The best-fit values obtained in the analysis are also used to construct the empirical relation RAR and BTFR.

RAR: The analysis of SPARC data shows that the total baryonic acceleration (a_{bar}) cannot explain the net observed acceleration (a_{obs}) and follow a certain analytical relation known as RAR [39]. This analysis has been found to be true for the 153 galaxies of the catalog irrespective of their morphological types, thus indicating a new dynamical law governing galaxy

kinematics. The empirical RAR relationship obtained from SPARC is defined as [39]

$$a_{obs}(R) = \frac{a_{bar}(R)}{1 - \exp(-\sqrt{a_{bar}(R)/a_*})}, \quad (3.2)$$

where a_* is the acceleration scale parameter and has best-fit value $a_* = 1.2 \times 10^{-10} \text{ ms}^{-2}$. For a rotationally supported galaxy, the net centripetal acceleration is defined in terms of observed velocity in SPARC catalog

$$a_{obs}(R) = \frac{v_{obs}^2(R)}{R} = \left| \frac{\partial \phi_{tot}(R)}{\partial R} \right|, \quad (3.3)$$

where ϕ_{tot} is the total potential i.e., total force per unit mass acting on a point particle. Similarly, $a_{bar}(R)$ is the linear sum of the acceleration for different baryonic components (disk, gas, and bulge) within the galaxy and can be estimated from the SPARC data using

$$a_{bar}(R) = \frac{v_N^2(R)}{R} = \frac{\gamma_d v_{disk}^2(R) + \gamma_b v_{bulge}^2(R) + |v_{gas}(R)| v_{gas}(R)}{R} = \left| \frac{\partial \phi_{bar}(R)}{\partial R} \right|. \quad (3.4)$$

Both the net circular velocity ($v_{obs}(r)$) and individual baryonic components mentioned in Eq.3.3 and 3.4 are known observationally in SPARC. This makes the relation an empirical one as it assumes no prior knowledge about the DM or MOG model and is purely from the observational data in SPARC.

For our analysis, we aim to probe RAR in the context of the RGGR gravity. The analytical expression for the net acceleration (Eq.2.5) in RGGR includes a $\bar{\nu}$ dependent extra component to the Newtonian part. As explained in the previous discussion in the context of RC, the best-fit value of this $\bar{\nu}$ parameter for each galaxy can be estimated from the circular velocity fitting with the SPARC data. Thus, the consistency of the RGGR predicted net acceleration (a_{RGGR}) with respect to the $a_{obs}(R)$ can be probed by the RAR. In the following, we compare the observed RAR with the same empirical relation Eq.3.2 in the context of the RGGR model for each data point of the qualifying SPARC galaxies.

BTFR: SPARC also shows a tight correlation between the dynamics of the galaxy with the baryonic distribution. BTFR suggests that the stellar mass of the galaxy has a power law dependence on the flat part of the circular velocity,

$$M_{bar} = AV_f^x. \quad (3.5)$$

Here M_{bar} refers to the baryonic mass contained within the galaxy and V_f is the velocity measured along the flat part of the RC. The optimal value of the free parameters (A, x) are obtained from the study of the SPARC catalog, and are estimated to be $A = 50 M_\odot \text{ km}^{-4} \text{ s}^4$, $x = 4$ [46]. Similar to RAR, BTFR is also known to be empirical in nature as it assumes no underlying gravity model and is strictly obtained from the SPARC data. For every galaxy in SPARC, the baryonic mass is the linear sum of disk, bulge, and gas components. For the RGGR model, the total circular velocity is estimated by V_{RGGR} (Eq.2.4) and is dependent on the free parameters ($\gamma_d, \gamma_b, \bar{\nu}$) which are already constrained using the observed RC of the galaxy. Thus, the V_f for the RGGR will also get modified. The relation between the M_{bar} and the RGGR predicted flat velocity for each qualifying SPARC galaxy should follow observed BTFR. This additional check for RGGR is crucial for the gravity model to remain phenomenologically consistent.

4 Methodology

Using the RC data for the qualifying SPARC galaxies, we fit the model parameters considering RGGR as the underlying gravity model. These free parameters are constrained using the publicly available *emcee* package [38] in PYTHON. This package works on the principle of Markov Chain Monte Carlo (MCMC), which samples the posterior distribution of the free model parameters. For a given observational data set \mathcal{D} , the posterior probability $\mathcal{P}(\theta|\mathcal{D})$ for unknown set of parameters θ is defined as

$$\mathcal{P}(\theta|\mathcal{D}) \propto \mathcal{L}(D|\theta)\pi(\theta), \quad (4.1)$$

where $\mathcal{L}(D|\theta)$ is the likelihood which determines the probability of a data for a given model with free parameters, and $\pi(\theta)$ represents the priors imposed on the free parameters. Assuming that the errors on the observed circular velocity follow a Gaussian distribution, the likelihood for each galaxy is written as

$$\mathcal{L}_g = (2\pi)^{-n/2} \left\{ \prod_{i=1}^n \sigma(r_i)^{-1} \right\} \exp \left\{ -\frac{1}{2} \sum_{i=1}^n \left(\frac{v_{g,obs}(r_i) - v_{tot}(r_i, \theta)}{\sigma(r_i)} \right)^2 \right\}, \quad (4.2)$$

here n represents the number of observational data points over which the likelihood is summed. Also, $v_{obs}(r)$ and $\sigma(r)$ are the total circular velocity and error on the observations defined at each radial point within the SPARC catalog. The analytical velocity $v_{tot}(r, \theta)$ computed at a certain radius for a given set of free parameters is given in Eq.2.5. The velocity contribution $v_{tot}(r, \theta)$ is dependent on free parameters, which are phenomenologically constrained by comparing with the observational circular velocity. The unknown parameters include the normalization mass-to-light factor (γ) introduced for the baryonic component i.e., disk and bulge of the galaxy, respectively. v_{tot} is also dependent on the model parameter \bar{v} . Thus, θ is composed of $\{\gamma_d, \gamma_b, \bar{v}\}$ which are to be estimated independently for each galaxy.

Regarding the $\pi(\theta)$, we assume flat priors for the model parameters. The mass-to-light ratio for both disk (γ_d) and bulge (γ_b) are assumed to have no radial dependence on the galaxy and are varied in the range [0.3, 0.8] [36, 47, 48]. Additionally, for the mass-dependent parameter \bar{v} , a wide range of parameter space is looked into and is varied within $10^{-9} \leq \bar{v} \leq 10^{-6}$. This range is motivated from the previous analysis of spiral and elliptical galaxies where \bar{v} is found to vary in order of 10^{-7} [29]. To ensure the convergence of the chain, we run the sampler for a sufficient number of steps such that the acceptance fraction lies within the range 0.3 – 0.5 [38]. Additionally, by estimating the autocorrelation time (τ) for each galaxy, we discard τ number of steps as burn-in before performing posterior analysis. We run a sufficient number of steps i.e., 50τ as specified in *emcee* [38], such that convergence is achieved.

Certain selection criteria are also adopted before choosing a galaxy from the SPARC catalog. This includes galaxies with asymmetrical RC i.e., $Q > 2$, and face-on galaxies having $i < 30^\circ$ which are exempted from our analysis [33]. Additionally, to ensure that we have a consistent RC fit, we reject galaxies whose goodness of fit i.e., $\chi_{red}^2 \geq 6$. The last quality cut is imposed manually to ensure a consistent fit for the model with the observations.

5 Results

In the following, we analyze the consistency of the RGGR framework with the observational circular velocity for our selection of SPARC galaxies. The RC analysis is done for galaxies belonging to different morphological types. The free model parameters are constrained using the emcee sampler scanning the parameter space to evaluate the best-fit values. For this, we look into the rotation curves of individual galaxies present within SPARC. Additionally, we also study the mass-dependent nature of the phenomenological parameter \bar{v} . These best-fit values must also satisfy the fundamental relationships RAR and BTFR, hence we compare our results for the RGGR model with both these relationships.

Table 1: The best-fit parameters obtained from the emcee sampler. Corresponding to the RGGR gravity model, for every galaxy, there are 3 parameters ($\gamma_d, \gamma_b, \bar{v}$) that are statistically constrained from the observed circular velocity.

Galaxy Name	Galaxy type	γ_d	γ_b	$\bar{v} \times 10^7$	χ_{red}^2
NGC7814	Early	0.53	0.31	7.23	1.18
NGC4138	Early	0.58	0.50	1.58	0.56
UGC02487	Early	0.80	0.79	8.26	4.07
UGC06614	Early	0.52	0.32	3.60	1.00
UGC03546	Early	0.59	0.34	2.15	0.90
UGC03205	Early	0.55	0.80	3.42	4.82
UGC08699	Early	0.69	0.51	1.61	1.40
UGC11914	Early	0.30	0.74	6.11	1.68
UGC06786	Early	0.39	0.55	4.33	2.28
NGC1090	Spiral	0.54	-	1.65	2.85
NGC2683	Spiral	0.56	0.54	1.88	0.69
NGC2841	Spiral	0.78	0.79	5.61	1.86
NGC3769	Spiral	0.33	-	1.41	0.91
NGC2955	Spiral	0.32	0.56	4.69	4.89
NGC4013	Spiral	0.30	0.37	2.53	2.38
NGC0801	Spiral	0.57	–	1.88	5.80
NGC5005	Spiral	0.46	0.35	3.68	0.13
NGC6195	Spiral	0.31	0.56	4.16	2.17
NGC7331	Spiral	0.30	0.36	3.61	2.00
UGC12506	Spiral	0.79	-	4.40	3.74
UGC11455	Spiral	0.41	-	5.09	4.16
UGC09037	Spiral	0.30	-	1.83	3.18
UGC07151	Spiral	0.78	-	0.39	2.39
UGC06983	Spiral	0.79	-	1.09	2.42
NGC4559	Spiral	0.41	-	0.70	1.02
NGC4100	Spiral	0.63	-	1.89	2.11
NGC4088	Spiral	0.31	-	1.62	1.10
NGC4085	Spiral	0.32	-	1.13	3.05
NGC3972	Spiral	0.68	-	1.26	2.01

Continued on next page

Table 1 – continued from previous page

Galaxy Name	Galaxy type	γ_d	γ_b	$\bar{\nu} \times 10^7$	χ_{red}^2
NGC3893	Spiral	0.38	-	2.48	0.53
NGC2998	Spiral	0.67	-	2.53	2.47
NGC0100	Spiral	0.32	-	1.05	0.63
ESO079-G014	Spiral	0.77	-	2.21	3.85
NGC0289	Spiral	0.65	-	2.27	1.89
NGC2976	Spiral	0.54	-	0.93	0.50
NGC3521	Spiral	0.44	-	2.22	0.76
NGC3949	Spiral	0.39	-	1.39	0.52
NGC3953	Spiral	0.75	-	0.76	0.55
NGC3992	Spiral	0.76	-	3.65	1.87
NGC4051	Spiral	0.64	-	0.31	1.30
NGC4183	Spiral	0.79	-	0.88	1.61
NGC4010	Late-type	0.36	-	1.42	1.44
NGC0300	Late-type	0.69	-	0.74	0.76
UGC04278	Late-type	0.79	-	0.75	3.46
UGC05721	Late-type	0.76	-	0.71	2.26
NGC7793	Late-type	0.64	-	0.53	0.64
UGC06446	Late-type	0.79	-	0.77	4.34
UGC07603	Late-type	0.37	-	0.48	0.61
UGC06930	Late-type	0.77	-	0.84	1.54
UGC08550	Late-type	0.79	-	0.30	3.87
UGC12732	Late-type	0.79	-	0.89	5.93
UGC11557	Late-type	0.35	-	0.38	0.84
UGC08490	Late-type	0.78	-	0.61	0.54
UGC07089	Late-type	0.45	-	0.51	0.13
UGC07261	Late-type	0.68	-	0.59	0.92
UGC07323	Late-type	0.60	-	0.56	0.21
UGC07399	Late-type	0.75	-	1.21	2.64
UGC06399	Late-type	0.73	-	0.71	0.51
UGC06917	Late-type	0.75	-	0.94	1.63
UGC05986	Late-type	0.39	-	1.79	1.02
UGC04499	Late-type	0.76	-	0.39	1.89
NGC3109	Late-type	0.51	-	0.53	0.89
NGC0055	Late-type	0.34	-	0.51	1.15
ESO116-G012	Late-type	0.66	-	0.90	1.88
IC2574	Late-type	0.42	-	0.44	2.73
UGCA444	Starburst	0.70	-	0.10	0.81
UGC08837	Starburst	0.43	-	0.17	0.48
UGC07559	Starburst	0.46	-	0.12	0.30
UGC07690	Starburst	0.71	-	0.25	0.38
UGC07866	Starburst	0.56	-	0.12	0.21
UGC06923	Starburst	0.48	-	0.49	0.77

Continued on next page

Table 1 – continued from previous page

Galaxy Name	Galaxy type	γ_d	γ_b	$\bar{v} \times 10^7$	χ_{red}^2
UGC05414	Starburst	0.50	-	0.36	0.08
UGC05829	Starburst	0.77	-	0.37	2.14
NGC4068	Starburst	0.41	-	0.12	0.23
NGC3741	Starburst	0.73	-	0.30	2.62
ESO444-G084	Starburst	0.66	-	0.32	1.08
KK98-251	Starburst	0.60	-	0.10	0.36

5.1 Fit to the observed Rotation Curve

Fitting the RC of each SPARC galaxy with the RGGR gravity model constrains the free parameters. It includes two mass modeling parameters defined for the baryonic component of a galaxy i.e., γ_d and γ_b . The additional model parameter, i.e., \bar{v} , comes from the choice of RGGR gravity and has been found to have an almost linear dependence on the luminous mass of the galaxy. We analyze the behavior of the phenomenological parameter \bar{v} with the baryonic mass for the large sample of SPARC galaxies. In particular, we study the consistency of the RGGR governed model for all four morphological types of the galaxies present in SPARC. This compares the phenomenological consistency of the RGGR gravity for all the different galaxy types.

Early-type galaxies

The first category belongs to the early-type galaxies, which can be identified from the presence of a bulge at the center and tight indistinguishable spiral arms in the outer parts of the disk. From the whole set of early-type, we analyze 9 galaxies that satisfy the selection criteria. Out of these 9 galaxies, we illustrate the RC fitting for 4 of them in Fig.1. This includes NGC7814 shown in the upper left panel, NGC4138 in the upper right, UGC06614 in the lower left, and UGC03546 in the lower right panel of Fig.1. For each galaxy shown, the grey dots with green error bars represent the observational total circular velocity traced by the HI component within the galaxy. We also plot the individual baryonic components i.e., disk, bulge, and gas, for each galaxy using the gray lines. The dashed gray line represents the radial variation of the gas velocity. The disk and bulge components of the galaxy scaled by their respective mass-to-light ratio are shown via. the dashed-dotted and dotted lines, respectively.

In particular, the first panel at the top left shows the RC for NGC7814. The constraints on the free parameters (γ_d, γ_b and $\bar{v} \times 10^7$) obtained from our analysis give 0.53, 0.31 and 7.23, respectively. The radial variation of the circular velocity (Eq.2.4) in the RGGR model with these best-fit parameters is plotted using a solid black line. The obtained value of χ_{red}^2 for the galaxy is 1.18 indicating a good fit to the observational data of NGC7814. Similarly, the obtained value of parameters and goodness of fit for the other early-type galaxies in the panel can be found in Table.1. The measured goodness of fit for the early-type galaxies as compiled in Table.1 points to positive results towards the RGGR model.

Spiral-type galaxies

The second class of galaxies mentioned in SPARC belongs to the Spiral type. One example of such a galaxy is our own Milky Way. Such galaxies are characterized by the presence of distinct spiral structures at the outer parts of the disk. Additionally, the bulge at the center is of comparatively smaller size. SPARC has a large collection of spiral galaxies and our

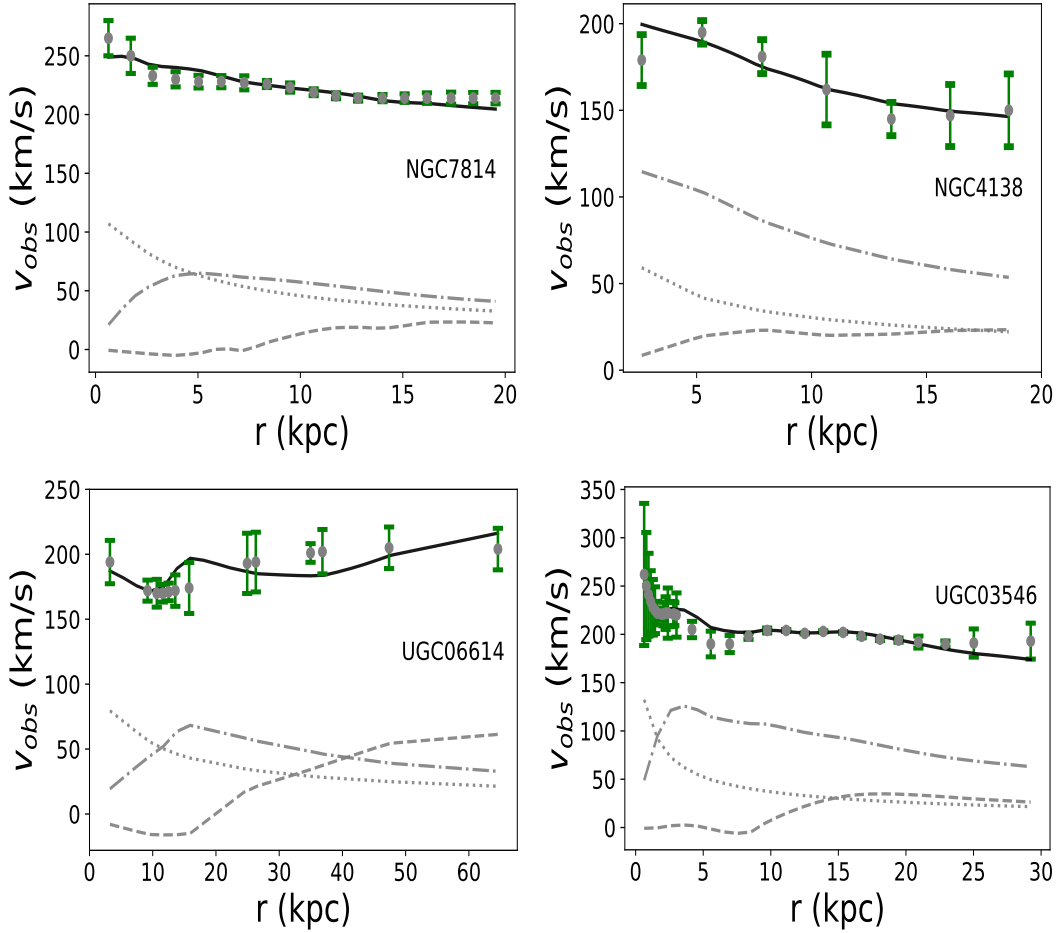


Figure 1: For Early-type galaxies the RC for 4 specimen galaxies are shown in the four panels above. The black solid line is the circular velocity when RGGR gravity contributes in addition to the baryonic part. The black dots with green error bars are the circular velocity data obtained from SPARC [33]. The dashed grey line represents the gaseous component of the galaxy. The dot-dashed line shows the variation of disk velocity within the galaxy, and the bulge part is plotted via the dotted line.

selection criteria gives us 39 such galaxies. Similar to Fig.1 we show 4 representative galaxies i.e., NGC1090, NGC2683, NGC2841 and NGC3769 in Fig.2. Out of the 4 galaxies shown, only two have a visible bulge component present and are represented by a dotted gray line in the plot. The gray points with error bars represent the total circular velocity observed in SPARC. Similarly, the gray lines represent the individual baryonic components in a galaxy.

The best fit parameters for the first subplot for NGC1090 shown at the top left panel in Fig.2 are $\gamma_d = 0.54$ and $\bar{v} \times 10^7 = 1.65$ with χ_{red}^2 equal to 2.85. For the obtained parameters, the net contribution to the total circular velocity, which is the sum of baryonic and RGGR components, is shown by a solid black line. The goodness of fits evaluated for each galaxy as given in Table.1 show that the RGGR model is a consistent choice in explaining the observed circular velocity of the spiral SPARC galaxies.

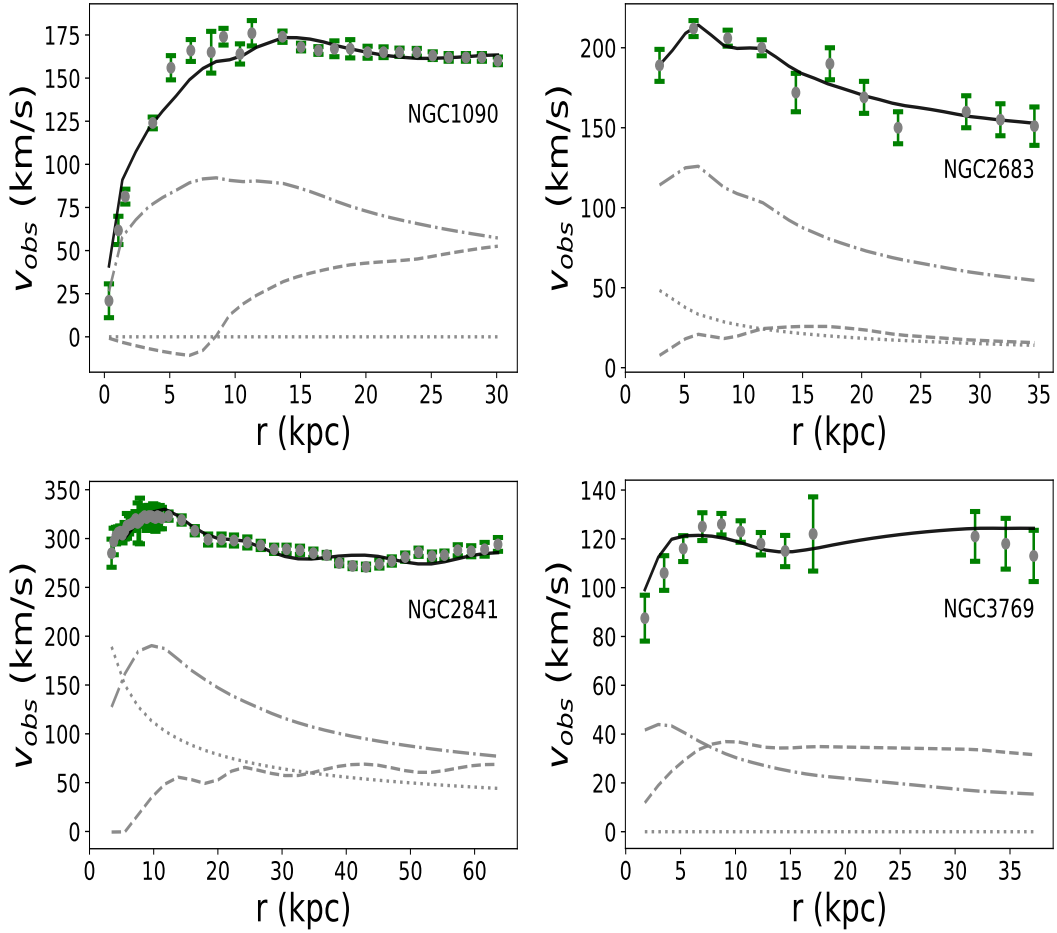


Figure 2: For Spiral-type galaxies, the RC for 4 specimen galaxies are shown in the panel. The black solid line is the circular velocity when RGGR gravity contributes in addition to the baryonic part. The black dots with green error bars are the circular velocity data obtained from SPARC [33]. The dashed grey line represents the gaseous component of the galaxy. The dot-dashed line shows the variation of disk velocity within the galaxy, and the bulge part is plotted via the dotted line.

Late-type dwarf

The third category of galaxies belongs to late-type dwarf, where the bulge is too faint to be observed. Thus, the baryonic component of the galaxy mostly constitutes disk and gas only. From the total late-type dwarf galaxies in the catalog, 34 galaxies fulfill the selection criteria. Similar to the above two categories, we plot four late-type dwarf galaxies in Fig.3. The galaxies that are illustrated include NGC4010 (top-left), NGC0300 (top-right), UGC04278 (bottom-left), and UGC05721 (bottom-right). The details on the plot corresponding to the observed circular velocity of a galaxy and its baryonic components follow the same convention as mentioned in the discussion of the previous two types of galaxies.

The circular velocity in the RGGR framework can be obtained by substituting the best-fit values of the model parameters i.e., $(\gamma_d, \gamma_b, \bar{v})$ as given in Table.1 in Eq.2.4. This radial variation is shown using the solid black line in Fig.2. The χ_{red}^2 computed in Table.1 for all

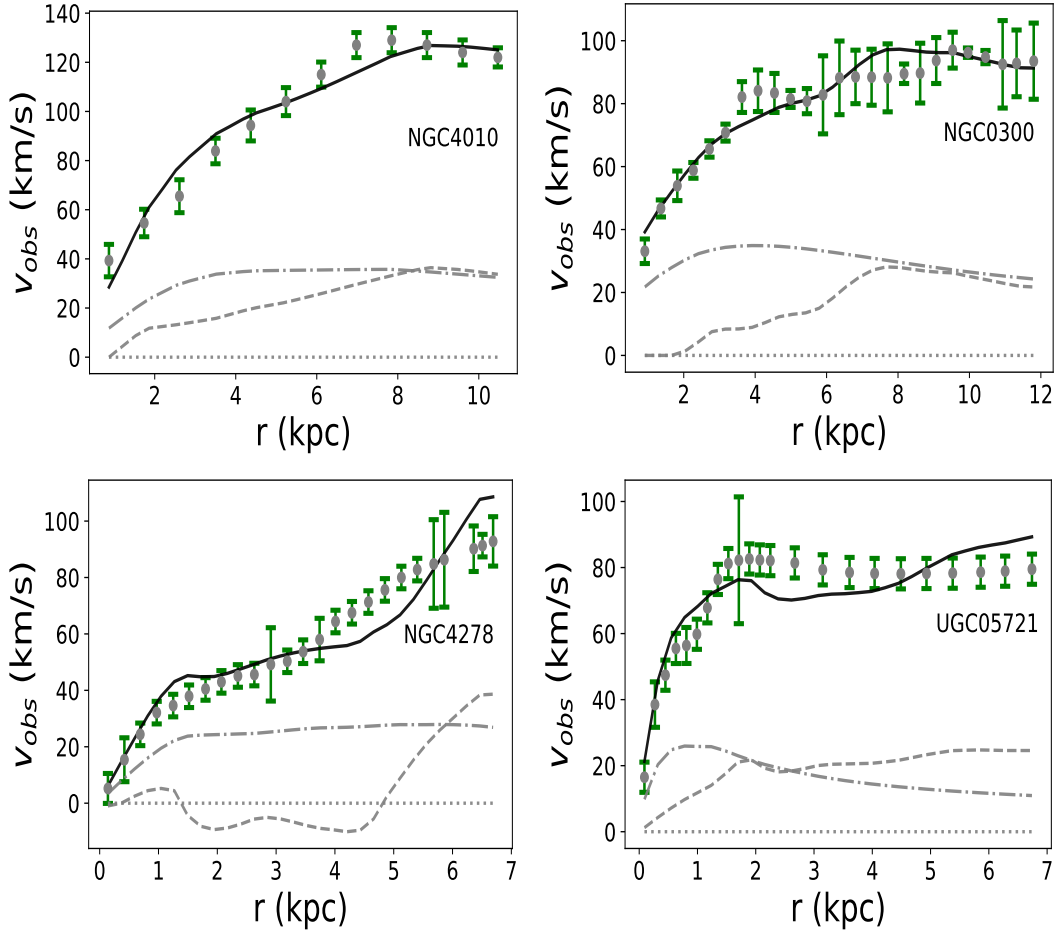


Figure 3: For Late-type galaxies, the RC for 4 specimen galaxies are shown in the panel. The black solid line is the circular velocity when RGGR gravity contributes in addition to the baryonic part. The black dots with green error bars are the circular velocity data obtained from SPARC [33]. The dashed grey line represents the gaseous component of the galaxy. The dot-dashed line shows the variation of disk velocity within the galaxy, and the bulge part is plotted via the dotted line.

the galaxies shows that the late-type dwarfs are a good fit with the RGGR model. This consistent behavior can also be visualized from the four sample plots shown in Fig.3.

Starburst galaxy

The fourth morphological type belongs to starburst galaxies which are relatively young with a high star formation rate. Such galaxies are dominated by gas and thus make a versatile region to look for the signature of the alternative gravity model. The morphology of such systems shows a diffused structure with no visible bulge and spiral arms. We studied 18 galaxies belonging to this particular morphological type and found that RGGR can give consistent fits with the observed circular velocities. As an illustration following the convention used in other morphological types, we plot 4 starburst galaxies i.e., UGC08837, UGC07559, UGC07690, and UGC07866 in Fig.4. The baryonic contribution for these types of galaxies comes from the gas and disk component only, as starbursts have no visible bulge present within. This

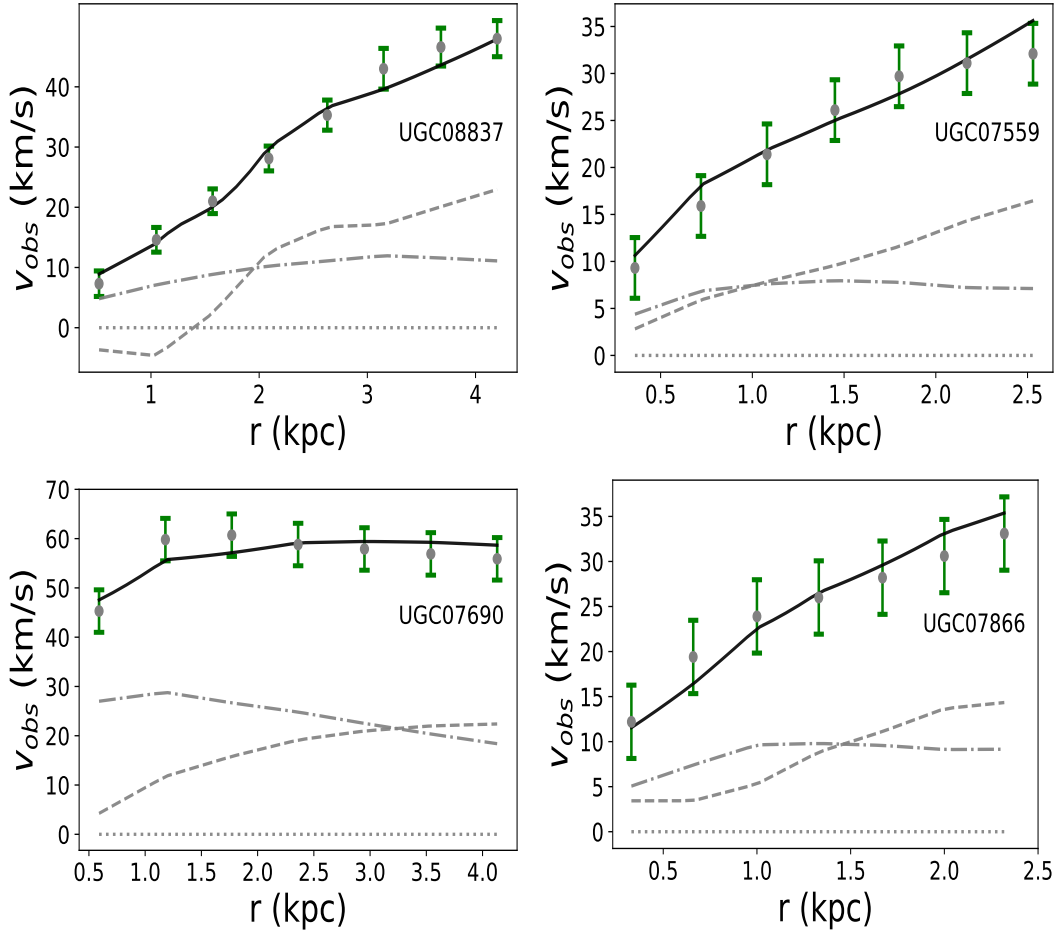


Figure 4: For Starburst galaxies, the RC for 4 specimen galaxies are shown in the panel. The black solid line is the circular velocity when RGRG gravity contributes in addition to the baryonic part. The black dots with green error bars are the circular velocity data obtained from SPARC [33]. The dashed grey line represents the gaseous component of the galaxy. The dot-dashed line shows the variation of disk velocity within the galaxy, and the bulge part is plotted via the dotted line.

is represented in the above plot by gray lines following the same convention used in preceding cases. Also, the total observed circular velocity with error bars is shown using gray points.

The constrained free parameters ($\gamma_d, \gamma_b, \bar{\nu} \times 10^7$) obtained for the aforementioned galaxies can be referred from Table.1. From the obtained values of parameters, the total circular velocity evaluated for each galaxy is shown by a solid black line in Fig.4. As can be seen from the plots, the observational circular velocity fits well with the analytical velocity in all 4 cases. Similarly, this consistent nature of the gravity model can also be quantified for all the starburst galaxies from the goodness of fit as mentioned in Table.1.

For the four different morphological types of galaxies discussed above, we find that RGRG is a phenomenologically consistent theory of gravity. The best fit values for the $\bar{\nu}$ parameter lies in the range $10^{-6} - 10^{-8}$. The parameters γ_d and γ_b fall in the range $0.3 - 0.8$, consistent with

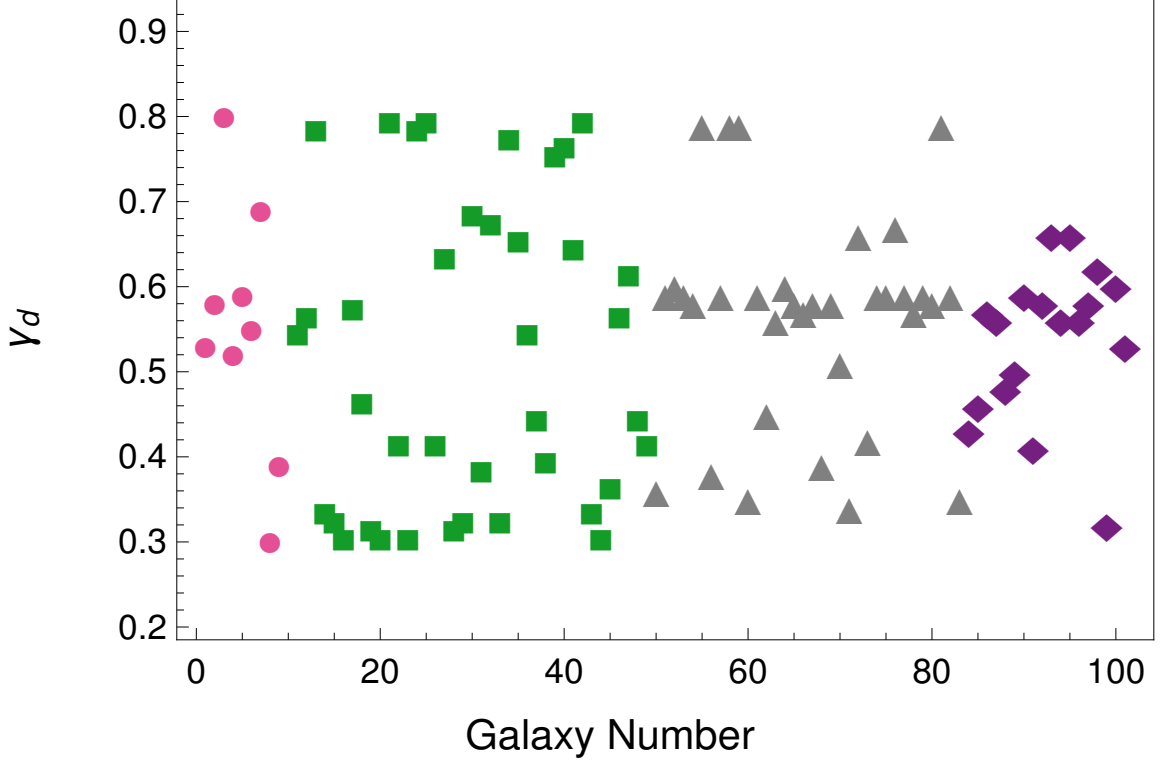


Figure 5: The plot shows the variation of γ_d . The varying morphological types are represented using different markers. The square markers represent the early type, and the circles are for the spiral galaxies. Additionally, γ_d for late-type and starburst are shown via triangle and diamond markers.

the choices of our priors. We also observe from Table.1 that the values of $\bar{\nu}$ are larger (in the range close to 10^{-6}) for the early-type galaxies compared to the other types. Interestingly, the $\bar{\nu}$ values decrease as we go across the Hubble type towards the late-type galaxies with $\bar{\nu}$ around 10^{-8} . This relation between the parameter $\bar{\nu}$ and the galaxy type can be understood from the baryonic mass content of the galaxies and is discussed in the next subsection.

The mass modeling parameters constrained for each galaxy in our analysis also include γ_d and γ_b and are assumed to be a constant having no radial dependence. The bulge component is prominent and can be majorly seen only in the early-type galaxies. Therefore, we utilize the disk normalization factor to show the variation of γ_d for the galaxies of different morphological types. The plot containing the values of γ_d for the 100 galaxies present in our analysis is shown in Fig.5. The behavior of γ_d represents that this parameter varies throughout the range of $[0.3, 0.8]$ for all galaxies. The different markers on the plot belong to the different morphological types of galaxies present in SPARC. The pink points give the value of γ_d for early-type galaxies. Similarly, green square, grey triangles, and violet diamond shapes represent γ_d for the spiral, late-type, and starburst galaxies respectively. Additionally, looking into the behavior of $\bar{\nu}$ in Table.1, shows that as we go from early type to starburst galaxies, the magnitude of the phenomenological parameter decreases. Such behavior of $\bar{\nu}$ with the stellar mass of galaxies is studied in detail in the next subsection.

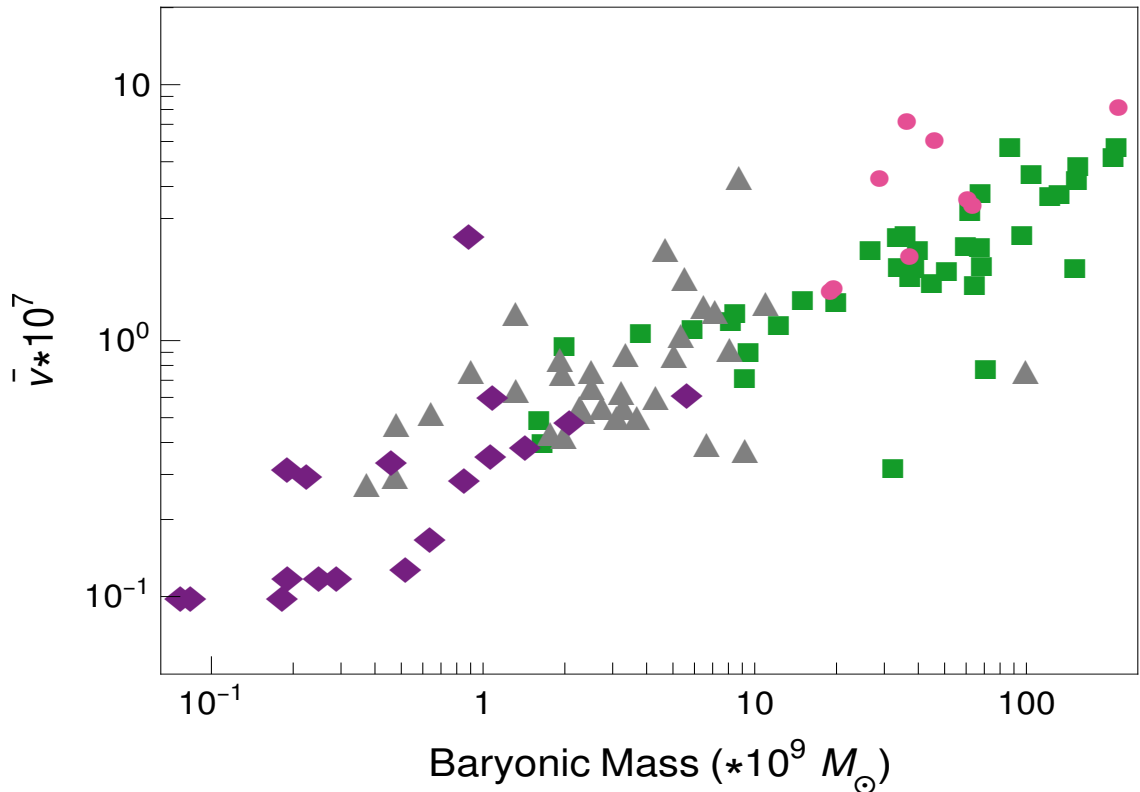


Figure 6: The plot relates the phenomenological parameter \bar{v} with the baryonic mass of the galaxy. The individual points are the representation of the \bar{v} evaluated for each galaxy studied in SPARC. The almost linear relation shown in the plot affirms the previous mass dependence claim for the RGGR parameter. The different markers in the plot show the different morphological types of galaxies, with the circle representing early-type, a square belonging to spiral, a triangle showing late-type dwarfs and a diamond for starburst galaxies.

5.2 Relation of \bar{v} with baryonic matter

To investigate the RGGR model parameter dependence on the baryonic mass, we rely on the same galaxies from the SPARC catalog. The baryonic mass of a rotationally supported galaxy consists of the bulge, disk, and gas components, as mentioned earlier. Each component of the galaxy (stellar+gas) is assumed to follow a distinct density distribution. The radial variation of matter distribution for disk and gas is assumed to vary exponentially [33, 42]. Similarly, for the galaxies having bulges, the density variation can be fitted with the Hernquist profile [43]. The total baryonic content for a galaxy is a linear mass sum of stellar and gas components. The galaxies in SAPRC constitute a wide range of masses varying from $10^8 - 10^{11} M_\odot$ [33]. For the scenario where the underlying gravity is assumed to be RGGR, the velocity contribution is the sum of the Newtonian part plus an additional term dependent on a free parameter (\bar{v}). This phenomenological parameter varies independently for each galaxy and is constrained from the study of RC as discussed in the previous section. A comparison of the constrained \bar{v} obtained along with the stellar mass of the galaxy is represented via an individual datapoint in Fig.6. The figure shows that the magnitude of the phenomenological parameter \bar{v} increases almost linearly with the increasing mass of the galaxies. Our analysis is thus justified with

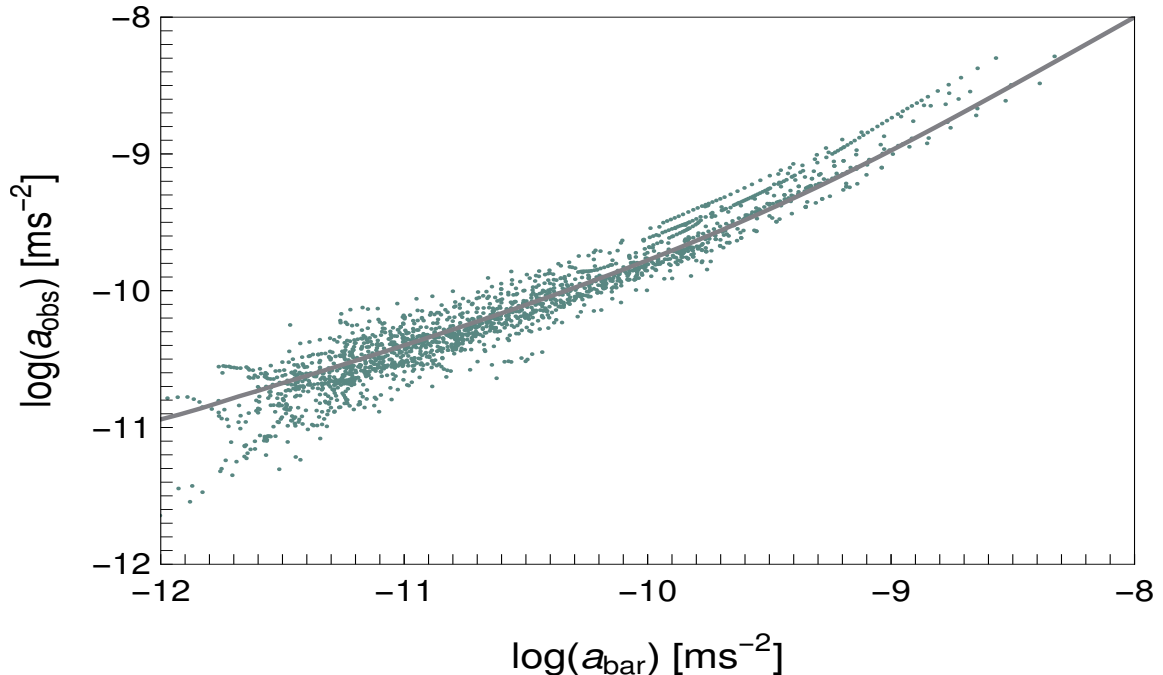


Figure 7: The plot compares the RAR relation where the total observed acceleration is evaluated in the RGGR framework. The black solid line shows the empirical relation Eq.(3.2) as obtained from the observations in SPARC. The green scatter points refer to the individual data points of all the galaxies analyzed where the net contribution to the acceleration gets modified as given by Eq.(2.5)

the previous study [29] done for the same gravity model. Different representations are used in the plot to categorize galaxies belonging to various morphological types. The pink round pointers belong to the early-type, the green square shows the spiral, the gray triangle is for the late-type, and the purple diamond represents the starburst galaxies. Clearly from the figure, we can see that the baryonic mass decreases from the early-type galaxies to the late-type ones, and accordingly, the value of $\bar{\nu}$ reduces linearly: a feature which can also be seen from the data provided in Table.1, i.e. $\bar{\nu}$ is smaller for the relatively younger galaxies. Such a linear relation of the model parameter with the mass of the system points towards the non-fundamental behavior of the RGGR model. However, as can be seen from the analysis of RC, the gravity model is consistent with the observations on astrophysical scales.

5.3 Empirical relations for SPARC

5.3.1 Radial Acceleration Relation (RAR)

The data points of the SPARC galaxies projecting the relation between the observed Eq.3.3 and baryonic acceleration Eq.3.4 is shown to follow an empirical relation as mentioned in Eq.3.2. This shows that in weak-gravity regions, the observed and baryonic acceleration follows the relation $a_{obs} \propto \sqrt{a_{bar}}$ and depends linearly in high acceleration scales as is expressed by the empirical relation. Thus, if RGGR is a consistent gravity model, it must satisfy RAR for the SPARC galaxies. This relation has been looked into and verified for a large sample of galaxies present in the SPARC catalog without any prior assumptions for the DM

or alternative gravity model. In the alternative gravity scenario, total circular velocity and acceleration are modified according to Eq.2.4 and Eq.2.5 respectively. The net acceleration is the sum of contribution coming from different baryonic components of a galaxy ($a_{bar}(r)$) with an additional part dependent on $\phi_N(r)$ and \bar{v} as expressed in Eq.2.5. In our analysis, we compare the modified acceleration ($a_{RGGR}(r)$) with $a_{bar}(r)$ to study the behavior of RAR in an alternative gravity framework.

The evaluation of the empirical relation requires the knowledge of free parameters, which is taken from the RC analysis in Sec.5.1. The RAR behavior as determined for the individual datapoint of all the selected galaxies in the RGGR framework is shown in Fig.7. The gray solid line is the analytical relation fitted from the observational data and has the form as given in Eq.2.5. Also, for each galaxy in our analysis, we determine the baryonic acceleration ($a_{bar}(r)$) at every radial point specified in the SAPRC catalog. Similarly, we also compute the RGGR acceleration ($a_{RGGR}(r)$) at every radial point. Thus, each green dot on the plot refers to the RGGR and baryonic acceleration at a specific radius for a given galaxy. The collection of points in Fig.7 contains the contribution for all the 100 galaxies selected in our analysis. Residual computed from the comparison of the relation with the 1840 data points, as illustrated in the figure, turns out to be 0.33 dex. Thus, from the best-fit parameters from the RC analysis, RAR behaves satisfactorily in the context of the RGGR model.

5.3.2 Baryonic Tully Fisher Relation (BTFR)

SPARC galaxies are also found to follow the BTFR (Eq.3.5), which provides a power law relation between the baryonic mass and the velocity measured at the flat part of the rotation curve. This relation holds irrespective of the gravity model. Therefore, for RGGR to be a consistent choice as an alternative gravity model, BTFR must be satisfied by the RGGR-predicted dynamics for the SPARC galaxies. To probe the BTFR,

$$\log(M_{bar}) = x \log(V_f) + \log A, \quad (5.1)$$

we consider the V_f corresponding to the RC fit with RGGR for each galaxy. The flat velocity (V_f) for each galaxy in the RGGR framework can be evaluated from the fit of the RC (Sec.5.1) at a given radius. The baryonic mass M_{bar} for a galaxy is a sum of stellar and gas components. The velocities of these different components are connected to their respective mass profile. For a given mass profile, M_{bar} can be estimated, particularly for the SPARC galaxies, the bulge and disk are assumed to have spheroidal and exponential distribution respectively [33]. BTFR has also been found to be sensitive on the radial choice [41] at which V_f is measured for SPARC galaxies. We evaluate the relation at $3.2 R_d$, which has shown an optimal behavior to the relation. The choice of $3.2 R_d$ [41, 49] ensures that 80% of the stellar matter is encompassed within the radius. Almost for all the SPARC galaxies we select, the distance of $3.2 R_d$ from the center of the galaxy corresponds to the flat region of the RC.

We use BayesLineFit package [41] which is based on *emcee* algorithm to find $(x, \log A)$. The best-fit value obtained for the parameters $(x, \log A)$ is found to be (3.55, 2.70) with an orthogonal scatter of 0.08 dex. We also report the vertical scatter given by [41]:

$$\sigma_0 = \sqrt{\frac{1}{n} \sum [\log(M_{bar}) - x \log(V_f) - \log A]^2}, \quad (5.2)$$

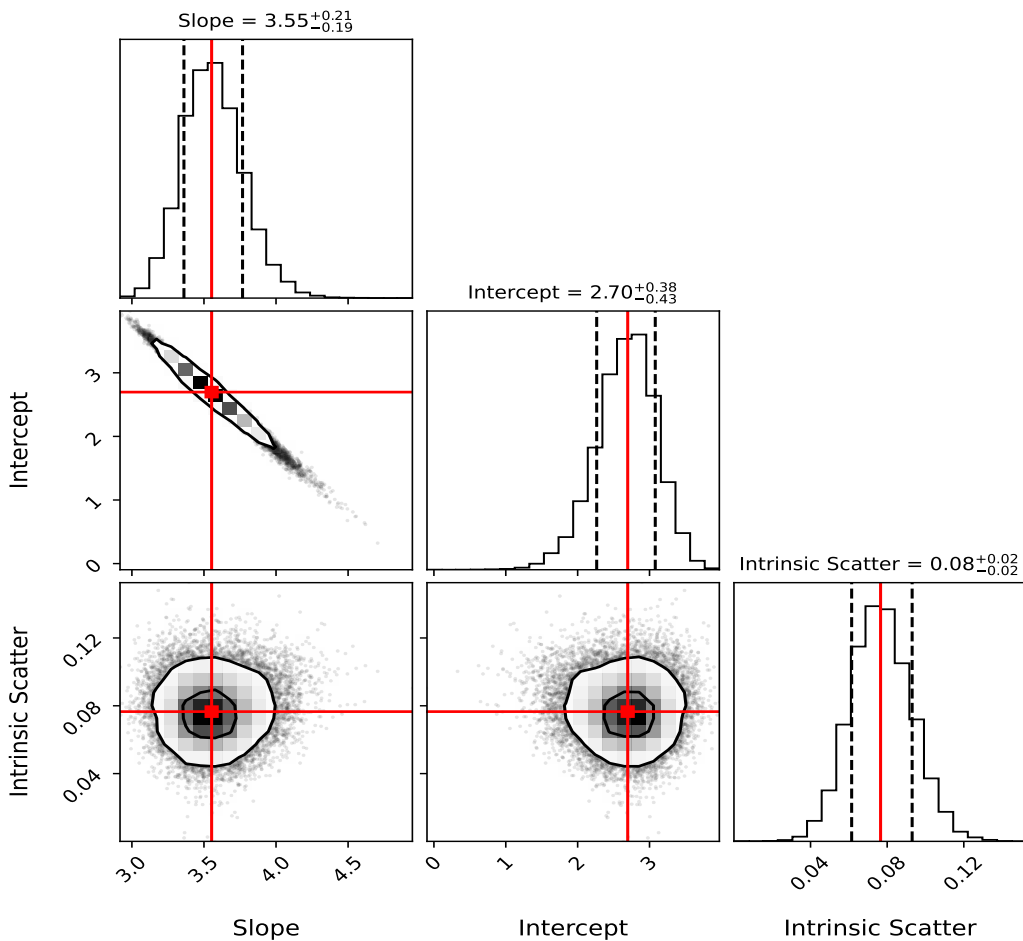


Figure 8: The posterior distribution of the parameter space in BTFR Eq.5.1 evaluated using BayesLineFit [41].

where n is the number of galaxies that are selected in our analysis. The observed σ_0 for the case of $3.2 R_d$ comes out to be 0.54. The posterior distribution for the fitting parameters i.e., slope (x), intercept ($\log A$), and intrinsic scatter, are shown in Fig.8. The solid red lines in the plot point towards the maximum likelihood values for the parameters. Given the best-fit parameters, BTFR for all the galaxies included in our analysis is illustrated in Fig.9. The solid gray circles represent the flat velocity for each SPARC galaxy evaluated at $r = 3.2 R_d$. Additionally, the green solid line shows a fit to the linear equation Eq.5.1 for the best-fit parameters obtained in our analysis. The BTFR plot in Fig.9 shows that the flat velocity evaluated at $3.2 R_d$ shows a consistent match with the observational results.

6 Conclusion

Our analysis focuses on the renormalization group improved gravity to explain the kinematics for a collection of rotationally supported galaxies compiled in the SPARC catalog. We, for the first time, study the dependence of the alternative gravity parameter on the galaxy morphology. We have looked into four different morphological types of galaxies, viz. early, spiral,

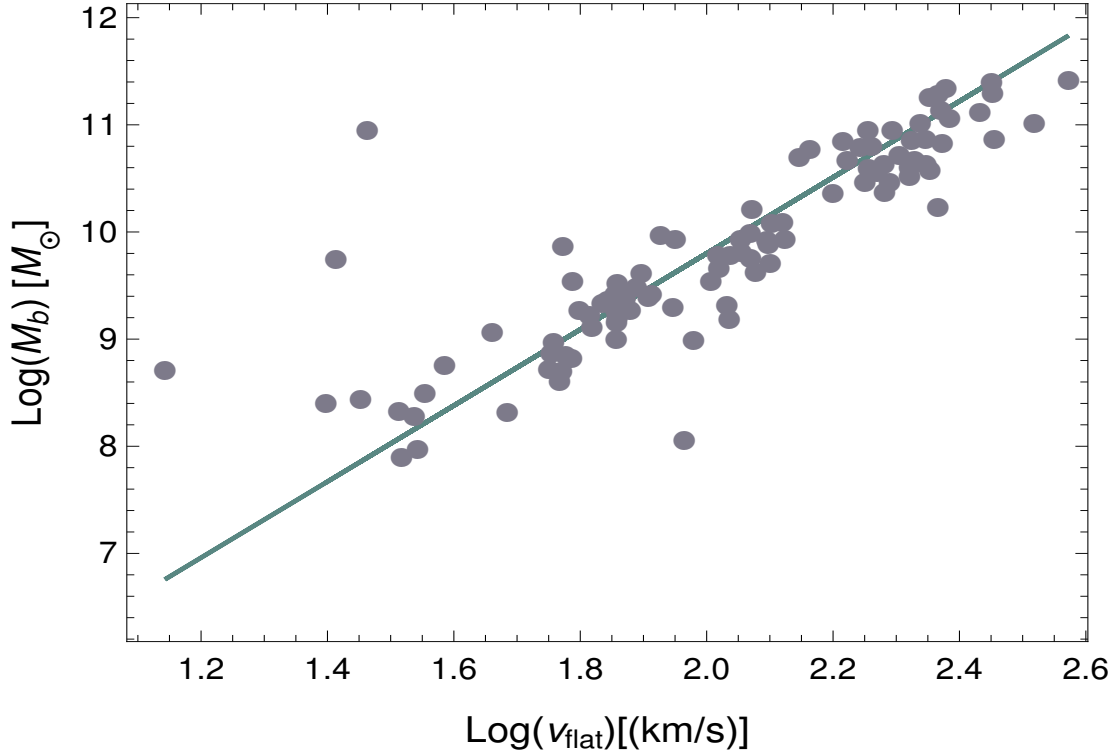


Figure 9: The BTFR with the flat circular velocity evaluated in RGGR model. The above plot estimates V_f for the RGGR model at $3.2 R_d$. The gray data points are the measure of flat velocity evaluated for individual galaxies. The green solid line shows the analytical best fit, consistent with the observed V_f in the RGGR framework.

late, and starburst. We have constrained the model parameter $\bar{\nu}$ for each galaxy taken from all four morphological types and have found that the RGGR consistently fits the observed net circular velocity. Our statistical analysis has probed this consistency for the individual galaxies using the goodness of fit. We have also checked the linear dependence of the model parameter $\bar{\nu}$ on the baryonic mass of the galaxy. The constrained values for the parameter $\bar{\nu}$ for our sample of the SPARC galaxies lie in the range $10^{-6} - 10^{-8}$ and are consistent with the variation of the masses of the galaxies under consideration. This implies that the older and heavier galaxies lead to a larger $\bar{\nu}$. Indeed, we have found that the parameter $\bar{\nu}$ decreases from the older galaxies to the younger ones.

We have further verified our goodness of fit from the RC analysis in light of the well-known empirical relations: RAR and BTFR. In particular, the RAR compares the radial variation of the observed and the baryonic acceleration. An additional factor comes in the baryonic acceleration due to the RGGR model. Our analysis has found that the RAR in the RGGR framework is in line with the established analytical relation obtained from previous observations. On a similar note, BTFR compares the baryonic mass with the observed flat velocity (V_f) of a galaxy, suggesting a power law dependence between them. The exact power law index has been found to be sensitive to the choice of the flat velocity radius. We have selected a radius of $3.2R_d$, which is known to show optimal behavior with the observations. Our analysis finds a tight correlation of the baryonic mass with flat velocity measured at $3.2R_d$ and has obtained a small orthogonal scatter of 0.08. This scatter may reduce even further for dif-

ferent choices of the radius of the V_f and by relieving the assumption of universal exponential density profile for the diffused gas component of the galaxy which requires further study.

An important aspect of the RGGR model is that the model parameter \bar{v} is dependent on the mass of the gravitating system. Many other alternative gravity models exhibit dependence of the model parameters on the scale of the system. Though this scale dependence of the phenomenological parameter may question the fundamental nature of these alternative gravity models, they may remain a consistent theory of gravity. Any alternative gravity model must satisfy the consistency criteria, i.e., it must be relativistic, self-consistent, and a complete theory free of ghosts and instabilities. The theory also requires to be able to explain the gravitational dynamics both in the strong and weak-field regimes as well as it should regain a valid Newtonian limit on the Solar System scales. RGGR thus remains a phenomenologically consistent theory of gravity and very importantly, satisfies the galactic kinematic observations for a large selection of SPARC galaxies.

Acknowledgments

Sovan Chakraborty acknowledges the support of the funding from DST-SERB projects CRG/2021/002961 and MTR/2021/000540. Sayan Chakrabarti would like to acknowledge the support from the DST-SERB research grant MTR/2022/000318. All the authors would like to acknowledge discussions and valuable inputs from Sayak Dutta. Esha Bhatia is indebted to the Ministry of Human Resource Development, Government of India, for assistance through a doctoral fellowship.

References

- [1] Timothy Clifton et al. “Modified Gravity and Cosmology”. In: *Phys. Rept.* 513 (2012), pp. 1–189. DOI: [10.1016/j.physrep.2012.01.001](https://doi.org/10.1016/j.physrep.2012.01.001). arXiv: [1106.2476](https://arxiv.org/abs/1106.2476) [[astro-ph.CO](#)].
- [2] Shin’ichi Nojiri and Sergei D. Odintsov. “Introduction to modified gravity and gravitational alternative for dark energy”. In: *eConf C0602061* (2006). Ed. by Andrzej Borowiec, p. 06. DOI: [10.1142/S0219887807001928](https://doi.org/10.1142/S0219887807001928). arXiv: [hep-th/0601213](https://arxiv.org/abs/hep-th/0601213).
- [3] F. Zwicky. “On the Masses of Nebulae and of Clusters of Nebulae”. In: *Astrophys. J.* 86 (1937), pp. 217–246. DOI: [10.1086/143864](https://doi.org/10.1086/143864).
- [4] Vera C. Rubin, W. Kent Ford Jr., and Norbert Thonnard. “Extended rotation curves of high-luminosity spiral galaxies. IV. Systematic dynamical properties, Sa through Sc”. In: *Astrophys. J. Lett.* 225 (1978), pp. L107–L111. DOI: [10.1086/182804](https://doi.org/10.1086/182804).
- [5] V. C. Rubin, N. Thonnard, and W. K. Ford Jr. “Rotational properties of 21 SC galaxies with a large range of luminosities and radii, from NGC 4605 /R = 4kpc/ to UGC 2885 /R = 122 kpc/”. In: *Astrophys. J.* 238 (1980), p. 471. DOI: [10.1086/158003](https://doi.org/10.1086/158003).
- [6] S. Nojiri, S. D. Odintsov, and V. K. Oikonomou. “Modified Gravity Theories on a Nutshell: Inflation, Bounce and Late-time Evolution”. In: *Phys. Rept.* 692 (2017), pp. 1–104. DOI: [10.1016/j.physrep.2017.06.001](https://doi.org/10.1016/j.physrep.2017.06.001). arXiv: [1705.11098](https://arxiv.org/abs/1705.11098) [[gr-qc](#)].
- [7] Leandros Perivolaropoulos and Foteini Skara. “Challenges for Λ CDM: An update”. In: *New Astron. Rev.* 95 (2022), p. 101659. DOI: [10.1016/j.newar.2022.101659](https://doi.org/10.1016/j.newar.2022.101659). arXiv: [2105.05208](https://arxiv.org/abs/2105.05208) [[astro-ph.CO](#)].
- [8] Anne M. Green. “Dark matter in astrophysics/cosmology”. In: *SciPost Phys. Lect. Notes* 37 (2022), p. 1. DOI: [10.21468/SciPostPhysLectNotes.37](https://doi.org/10.21468/SciPostPhysLectNotes.37). arXiv: [2109.05854](https://arxiv.org/abs/2109.05854) [[hep-ph](#)].

- [9] Mariia Khelashvili, Anton Rudakovskiy, and Sabine Hossenfelder. “Dark matter profiles of SPARC galaxies: a challenge to fuzzy dark matter”. In: *Mon. Not. Roy. Astron. Soc.* 523.3 (2023), pp. 3393–3405. DOI: [10.1093/mnras/stad1595](https://doi.org/10.1093/mnras/stad1595). arXiv: [2207.14165](https://arxiv.org/abs/2207.14165) [[astro-ph.CO](#)].
- [10] WJG De Blok et al. “The core-cusp problem”. In: *Advances in Astronomy 2010* (2010).
- [11] H. E. S. Velten, R. F. vom Marttens, and W. Zimdahl. “Aspects of the cosmological “coincidence problem””. In: *Eur. Phys. J. C* 74.11 (2014), p. 3160. DOI: [10.1140/epjc/s10052-014-3160-4](https://doi.org/10.1140/epjc/s10052-014-3160-4). arXiv: [1410.2509](https://arxiv.org/abs/1410.2509) [[astro-ph.CO](#)].
- [12] Anatoly A. Klypin et al. “Where are the missing Galactic satellites?” In: *Astrophys. J.* 522 (1999), pp. 82–92. DOI: [10.1086/307643](https://doi.org/10.1086/307643). arXiv: [astro-ph/9901240](https://arxiv.org/abs/astro-ph/9901240).
- [13] G Kauffmann, Simon D. M. White, and B. Guiderdoni. “The Formation and Evolution of Galaxies Within Merging Dark Matter Haloes”. In: *Mon. Not. Roy. Astron. Soc.* 264 (1993), p. 201.
- [14] Steven Weinberg. “The Cosmological Constant Problem”. In: *Rev. Mod. Phys.* 61 (1989). Ed. by Jong-Ping Hsu and D. Fine, pp. 1–23. DOI: [10.1103/RevModPhys.61.1](https://doi.org/10.1103/RevModPhys.61.1).
- [15] Jeremiah P. Ostriker and Paul J. Steinhardt. “New light on dark matter”. In: *Science* 300 (2003), pp. 1909–1913. DOI: [10.1126/science.1085976](https://doi.org/10.1126/science.1085976). arXiv: [astro-ph/0306402](https://arxiv.org/abs/astro-ph/0306402).
- [16] B. Moore. “Evidence against dissipationless dark matter from observations of galaxy haloes”. In: *Nature* 370 (1994), p. 629. DOI: [10.1038/370629a0](https://doi.org/10.1038/370629a0).
- [17] Shinji Tsujikawa. “Modified gravity models of dark energy”. In: *Lect. Notes Phys.* 800 (2010), pp. 99–145. DOI: [10.1007/978-3-642-10598-2_3](https://doi.org/10.1007/978-3-642-10598-2_3). arXiv: [1101.0191](https://arxiv.org/abs/1101.0191) [[gr-qc](#)].
- [18] Antonio De Felice, Mark Hindmarsh, and Mark Trodden. “Ghosts, Instabilities, and Superluminal Propagation in Modified Gravity Models”. In: *JCAP* 08 (2006), p. 005. DOI: [10.1088/1475-7516/2006/08/005](https://doi.org/10.1088/1475-7516/2006/08/005). arXiv: [astro-ph/0604154](https://arxiv.org/abs/astro-ph/0604154).
- [19] B. P. Abbott et al. “Binary Black Hole Mergers in the first Advanced LIGO Observing Run”. In: *Phys. Rev. X* 6.4 (2016). [Erratum: *Phys.Rev.X* 8, 039903 (2018)], p. 041015. DOI: [10.1103/PhysRevX.6.041015](https://doi.org/10.1103/PhysRevX.6.041015). arXiv: [1606.04856](https://arxiv.org/abs/1606.04856) [[gr-qc](#)].
- [20] Nicolás Yunes and Xavier Siemens. “Gravitational-Wave Tests of General Relativity with Ground-Based Detectors and Pulsar Timing-Arrays”. In: *Living Rev. Rel.* 16 (2013), p. 9. DOI: [10.12942/lrr-2013-9](https://doi.org/10.12942/lrr-2013-9). arXiv: [1304.3473](https://arxiv.org/abs/1304.3473) [[gr-qc](#)].
- [21] M. Reuter and H. Weyer. “Quantum gravity at astrophysical distances?” In: *JCAP* 12 (2004), p. 001. DOI: [10.1088/1475-7516/2004/12/001](https://doi.org/10.1088/1475-7516/2004/12/001). arXiv: [hep-th/0410119](https://arxiv.org/abs/hep-th/0410119).
- [22] Ilya L. Shapiro, Joan Sola, and Hrvoje Stefancic. “Running G and Lambda at low energies from physics at M(X): Possible cosmological and astrophysical implications”. In: *JCAP* 01 (2005), p. 012. DOI: [10.1088/1475-7516/2005/01/012](https://doi.org/10.1088/1475-7516/2005/01/012). arXiv: [hep-ph/0410095](https://arxiv.org/abs/hep-ph/0410095).
- [23] C. Farina et al. “Dynamics of the Laplace-Runge-Lenz vector in the quantum-corrected Newton gravity”. In: *Phys. Rev. D* 83 (2011), p. 124037. DOI: [10.1103/PhysRevD.83.124037](https://doi.org/10.1103/PhysRevD.83.124037). arXiv: [1101.5611](https://arxiv.org/abs/1101.5611) [[gr-qc](#)].
- [24] Davi C. Rodrigues, Patricio S. Letelier, and Ilya L. Shapiro. “Galaxy rotation curves from General Relativity with Renormalization Group corrections”. In: *JCAP* 04 (2010), p. 020. DOI: [10.1088/1475-7516/2010/04/020](https://doi.org/10.1088/1475-7516/2010/04/020). arXiv: [0911.4967](https://arxiv.org/abs/0911.4967) [[astro-ph.CO](#)].
- [25] Davi C. Rodrigues. “Elliptical galaxies kinematics within general relativity with renormalization group effects”. In: *JCAP* 09 (2012), p. 031. DOI: [10.1088/1475-7516/2012/09/031](https://doi.org/10.1088/1475-7516/2012/09/031). arXiv: [1203.2286](https://arxiv.org/abs/1203.2286) [[astro-ph.CO](#)].

- [26] Davi C. Rodrigues et al. “Disk and elliptical galaxies within renormalization group improved gravity”. In: *AIP Conf. Proc.* 1471 (2012). Ed. by Jailson Alcaniz et al., pp. 98–102. DOI: [10.1063/1.4756820](https://doi.org/10.1063/1.4756820). arXiv: [1209.0504](https://arxiv.org/abs/1209.0504) [[astro-ph.CO](#)].
- [27] Julio C. Fabris et al. “Quantum corrections to gravity and their implications for cosmology and astrophysics”. In: *Int. J. Mod. Phys. A* 27 (2012). Ed. by M. Asorey, M. Bordag, and Emilio Elizalde, p. 1260006. DOI: [10.1142/S0217751X12600068](https://doi.org/10.1142/S0217751X12600068). arXiv: [1203.2695](https://arxiv.org/abs/1203.2695) [[astro-ph.CO](#)].
- [28] Ilya L. Shapiro and Joan Sola. “Scaling behavior of the cosmological constant: Interface between quantum field theory and cosmology”. In: *JHEP* 02 (2002), p. 006. DOI: [10.1088/1126-6708/2002/02/006](https://doi.org/10.1088/1126-6708/2002/02/006). arXiv: [hep-th/0012227](https://arxiv.org/abs/hep-th/0012227).
- [29] Davi C. Rodrigues et al. “Modified gravity models and the central cusp of dark matter haloes in galaxies”. In: *Mon. Not. Roy. Astron. Soc.* 445.4 (2014), pp. 3823–3838. DOI: [10.1093/mnras/stu2017](https://doi.org/10.1093/mnras/stu2017). arXiv: [1409.7524](https://arxiv.org/abs/1409.7524) [[astro-ph.GA](#)].
- [30] Silvije Domazet and Hrvoje Stefancic. “Renormalization group scale-setting in astrophysical systems”. In: *Phys. Lett. B* 703 (2011), pp. 1–6. DOI: [10.1016/j.physletb.2011.07.038](https://doi.org/10.1016/j.physletb.2011.07.038). arXiv: [1010.3585](https://arxiv.org/abs/1010.3585) [[gr-qc](#)].
- [31] Ilya L. Shapiro et al. “Variable cosmological constant as a Planck scale effect”. In: *Phys. Lett. B* 574 (2003), pp. 149–155. DOI: [10.1016/j.physletb.2003.09.016](https://doi.org/10.1016/j.physletb.2003.09.016). arXiv: [astro-ph/0303306](https://arxiv.org/abs/astro-ph/0303306).
- [32] Paulo L. C. de Oliveira, J. A. Freitas Pacheco, and Gilbert Reinisch. “Testing two alternative theories to dark matter with the Milky Way dynamics”. In: *General Relativity and Gravitation* 47 (2015), pp. 1–16. URL: <https://api.semanticscholar.org/CorpusID:118410530>.
- [33] Federico Lelli, Stacy S. McGaugh, and James M. Schombert. “SPARC: Mass Models for 175 Disk Galaxies with Spitzer Photometry and Accurate Rotation Curves”. In: *Astron. J.* 152 (2016), p. 157. DOI: [10.3847/0004-6256/152/6/157](https://doi.org/10.3847/0004-6256/152/6/157). arXiv: [1606.09251](https://arxiv.org/abs/1606.09251) [[astro-ph.GA](#)].
- [34] Tao Ren et al. “Reconciling the Diversity and Uniformity of Galactic Rotation Curves with Self-Interacting Dark Matter”. In: *Phys. Rev. X* 9.3 (2019), p. 031020. DOI: [10.1103/PhysRevX.9.031020](https://doi.org/10.1103/PhysRevX.9.031020). arXiv: [1808.05695](https://arxiv.org/abs/1808.05695) [[astro-ph.GA](#)].
- [35] Aneesh P. Naik et al. “Constraints on Chameleon f(R)-Gravity from Galaxy Rotation Curves of the SPARC Sample”. In: *Mon. Not. Roy. Astron. Soc.* 489.1 (2019), pp. 771–787. DOI: [10.1093/mnras/stz2131](https://doi.org/10.1093/mnras/stz2131). arXiv: [1905.13330](https://arxiv.org/abs/1905.13330) [[astro-ph.CO](#)].
- [36] Álefe O. F. de Almeida, Luca Amendola, and Viviana Niro. “Galaxy rotation curves in modified gravity models”. In: *JCAP* 08 (2018), p. 012. DOI: [10.1088/1475-7516/2018/08/012](https://doi.org/10.1088/1475-7516/2018/08/012). arXiv: [1805.11067](https://arxiv.org/abs/1805.11067) [[astro-ph.GA](#)].
- [37] M. A. Green and J. W. Moffat. “Modified Gravity (MOG) fits to observed radial acceleration of SPARC galaxies”. In: *Phys. Dark Univ.* 25 (2019), p. 100323. DOI: [10.1016/j.dark.2019.100323](https://doi.org/10.1016/j.dark.2019.100323). arXiv: [1905.09476](https://arxiv.org/abs/1905.09476) [[gr-qc](#)].
- [38] Daniel Foreman-Mackey et al. “emcee: the MCMC hammer”. In: *Publications of the Astronomical Society of the Pacific* 125.925 (2013), p. 306.
- [39] Stacy S McGaugh, Federico Lelli, and James M Schombert. “Radial acceleration relation in rotationally supported galaxies”. In: *Physical Review Letters* 117.20 (2016), p. 201101.
- [40] R. B. Tully and J. R. Fisher. “A New method of determining distances to galaxies”. In: *Astron. Astrophys.* 54 (1977), pp. 661–673.
- [41] Federico Lelli et al. “The baryonic Tully–Fisher relation for different velocity definitions and implications for galaxy angular momentum”. In: *Mon. Not. Roy. Astron.*

- Soc.* 484.3 (2019), pp. 3267–3278. DOI: [10.1093/mnras/stz205](https://doi.org/10.1093/mnras/stz205). arXiv: [1901.05966](https://arxiv.org/abs/1901.05966) [[astro-ph.GA](#)].
- [42] K. C. Freeman. “On the disks of spiral and SO Galaxies”. In: *Astrophys. J.* 160 (1970), p. 811. DOI: [10.1086/150474](https://doi.org/10.1086/150474).
- [43] Lars Hernquist. “An Analytical Model for Spherical Galaxies and Bulges”. In: *The Astrophysical Journal* 356 (1990), pp. 359–364. URL: <https://api.semanticscholar.org/CorpusID:122140408>.
- [44] Esha Bhatia, Sayan Chakrabarti, and Sovan Chakraborty. “Velocity dispersion of dark-matter deficient ultradiffuse galaxies: A case for modified gravity”. In: *Phys. Rev. D* 108.6 (2023), p. 064021. DOI: [10.1103/PhysRevD.108.064021](https://doi.org/10.1103/PhysRevD.108.064021). arXiv: [2306.11790](https://arxiv.org/abs/2306.11790) [[gr-qc](#)].
- [45] D. Mihalas and J. Binney. *Galactic Astronomy: Structure and Kinematics*. W.H. Freeman, 1981. ISBN: 9780716712800. URL: <https://books.google.co.in/books?id=aT2fQgAACAAJ>.
- [46] Stacy S. McGaugh. “The Baryonic Tully-Fisher relation of galaxies with extended rotation curves and the stellar mass of rotating galaxies”. In: *Astrophys. J.* 632 (2005), pp. 859–871. DOI: [10.1086/432968](https://doi.org/10.1086/432968). arXiv: [astro-ph/0506750](https://arxiv.org/abs/astro-ph/0506750).
- [47] James Schombert and Stacy McGaugh. “Stellar populations and the star formation histories of LSB galaxies: III. Stellar population models”. In: *Publications of the Astronomical Society of Australia* 31 (2014), e036.
- [48] Sharon E. Meidt et al. “Reconstructing the stellar mass distributions of galaxies using S⁴G IRAC 3.6 and 4.5 μ m images: II. The conversion from light to mass”. In: *Astrophys. J.* 788 (2014), p. 144. DOI: [10.1088/0004-637X/788/2/144](https://doi.org/10.1088/0004-637X/788/2/144). arXiv: [1402.5210](https://arxiv.org/abs/1402.5210) [[astro-ph.GA](#)].
- [49] Aaron J Romanowsky and S Michael Fall. “Angular momentum and galaxy formation revisited”. In: *The Astrophysical Journal Supplement Series* 203.2 (2012), p. 17.